Coupled Systems Mechanics, *Vol. 9, No. 1 (2020) 63–75*
DOI: https://doi.org/10.12989/csm.2020.9.1.063

Towards isotropic transport with co-meshes

Christina Paulin[a], Éric Heulhard de Montigny[b] and Antoine Llor*

CEA, DAM, DIF, F-91297 Arpajon, France

(Received July 1, 2019, Revised December 11, 2019, Accepted December 12, 2019)

Abstract. Transport is the central ingredient of all numerical schemes for hyperbolic partial differential equations and in particular for hydrodynamics. Transport has thus been extensively studied in many of its features and for numerous specific applications. In more than one dimension, it is most commonly plagued by a major artifact: mesh imprinting. Though mesh imprinting is generally inevitable, its *anisotropy* can be modulated and is thus amenable to significant reduction.

In the present work we introduce a new definition of stencils by taking into account second nearest neighbors (across cell corners) and call the resulting strategy "co-mesh approach". The modified equation is used to study numerical dissipation and tune enlarged stencils in order to minimize transport anisotropy.

Keywords: transport; numerical diffusion; isotropy; mesh imprinting; modified equation

1. Introduction

Various existing techniques for reducing the anisotropy of numerical transport resort to either of two strategies: i) improve the order of accuracy of schemes, or ii) make mesh and discretization stencil more isotropic. In the latter approach, one can mention Lagrange-remap schemes for hydrodynamics, where so-called corner fluxes appear (Burton *et al.* 2015, Hirt *et al.* 1974), face centered cubic (FCC) or body-centered cubic (BCC) lattices, often used for 3D wave propagation and linear magneto-hydrodynamics (MHD) (Potter *et al.* 2011, Salmasi and Potter 2018, Hamilton and Bilbao 2013), isotropic finite-differences, to correct lowest order error terms (Kumar 2004), interfacial flux splitting, to reduce mesh-locking effects for the heterogeneous, anisotropic diffusion problem (Terekhov *et al.* 2017), flux-corrected transport (FCT), which treats mesh-imprinting issues to achieve vorticity preservation (Lung and Roe 2014), geometric correctors, to achieve consistency by constraining convergence to asymptotically regular meshes (Bouche *et al.* 2005), etc.

Motivated by the development of hydro-codes for Inertial Confinement Fusion (ICF), (Zohuri 2017), a novel multi-fluid multi-dimensional direct-ALE hydro-scheme approach was recently introduced (Vazquez-Gonzalez 2016). When deriving the scheme—designated as GEEC for Geometry, Energy, and Entropy Compatible—a critical step appeared to be the definition of a proper discrete

*Corresponding author, E-mail: antoine.llor@cea.fr
[a]E-mail: christina.paulin.ocre@cea.fr
[b]E-mail: eric.heulhard-de-montigny@cea.fr

http://www.techno-press.org/?journal=csm&subpage=8 ISSN: 2234-2184 (Print), 2234-2192 (Online)

transport operator. In its present (first-order) form, its displays a significant anisotropic behavior that requires improvement for effective usage in applications.

The present work thus aims at studying and reducing the 2D anisotropy of the discrete first-order transport scheme. For this purpose, we privilege strategy ii) above to improve isotropy before upgrading the transport operator to higher order. This is done with an enlarged first-order upwind stencil. Following strategy i) above would have introduced complexities in the quasi-symplectic design of the GEEC scheme due to corner fluxes without actually much improvement on anisotropy to second order.

This approach is inspired by the following quote from P. Roe: *"... respecting the correct propagation of information under all circumstances. This includes seeking modes of propagation that are isotropic when they should be."* (Roe 2017).

2. Generic form and properties of the discrete Eulerian transport operator

The Eulerian transport operator for a field a under velocity field $\boldsymbol{u}$ writes

$$\mathrm{D}_t a = \partial_t a + \boldsymbol{\nabla} \cdot (a\boldsymbol{u}). \tag{1}$$

In the ALE context (Arbitrary Lagrangian Eulerian) $\boldsymbol{u}$ is the velocity in the reference frame, defined by the sum of relative-to-grid velocity $\boldsymbol{v}$ and grid velocity $\boldsymbol{w}$, $\boldsymbol{u} = \boldsymbol{v} + \boldsymbol{w}$. Remark that by definition $\boldsymbol{v} = 0$ represents Lagrangian transport by field $\boldsymbol{w}$, whereas $\boldsymbol{w} = 0$ represents Eulerian transport by field $\boldsymbol{v}$.

The generic first-order conservative discretization of the linear Eulerian transport operator (1) writes

$$\mathrm{D}_{\Delta t} a_c^n = V_c^{n+1} a_c^{n+1} - V_c^n a_c^n + \Delta t^n \sum_{d \in \mathcal{D}(c)} \big(a_c^n \mathring{V}_{cd}^n - a_d^n \mathring{V}_{dc}^n \big), \tag{2}$$

where the transported field a is defined at cell center x_c as its average value over (moving mesh) cell c of volume V_c—$\mathcal{D}(c)$ being the set of cell labels logically connected to cell c, as defined by the stencil. In order to preserve linearity with respect to velocity, the volume transfer rates $\mathring{V}_{cd}^n$ must be linear forms of relative-to-grid velocities $\boldsymbol{v}_q^n$—which are given at some nodes q related but not necessarily identical to the grid nodes—most generally represented by vectors $\boldsymbol{s}_{cdq}^n$

$$\mathring{V}_{cd}^n := \sum_{q \in \mathcal{Q}(c)} \boldsymbol{v}_q^n \cdot \boldsymbol{s}_{cdq}^n, \tag{3}$$

—$\mathcal{Q}(c)$ being the set of nodes q logically connected to cell c.

Elementary analysis of stability and consistency constrain the features of the transport operator (2) as follows: i) for stability, transport must be upwinded with respect the velocity direction, i.e. $\boldsymbol{s}_{cdq}^n \cdot \boldsymbol{v}_q^n \geq 0$ in (3), and this makes $\mathring{V}_{cd}^n$ to be a piecewise linear function of the $\boldsymbol{v}_q^n$ or

$$\mathring{V}_{cd}^n := \sum_{q \in \mathcal{Q}(c)} \sigma_{cdq}^n \boldsymbol{v}_q^n \cdot \boldsymbol{s}_{cdq}^n, \qquad \text{where} \qquad \sigma_{cdq} := \mathrm{H}(\boldsymbol{v}_q \cdot \boldsymbol{s}_{cdq}), \tag{4}$$

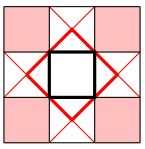

Fig. 1 Cell with its first nearest neighbors (white) and its co-cell boundaries connected to second nearest neighbors (pink).

H being the Heaviside function ($\mathrm{H}(0) = 1/2$ is assumed); ii) to avoid the DeBar artifact (DeBar 1974), velocities $\boldsymbol{v}_q$ must be collocated with transported field a_c, i.e. only one point $\boldsymbol{x}_q = \boldsymbol{x}_c$ is associated to any $\mathring{V}^n_{cd}$ in (3) and $\boldsymbol{s}_{cdq}$ reduces to $\boldsymbol{s}_{cd} := \boldsymbol{s}_{cdc}$

$$\mathring{V}^n_{cd} := \sigma^n_{cd} \boldsymbol{v}^n_c \cdot \boldsymbol{s}^n_{cd}; \tag{5}$$

iii) consistency to first order with the continuous formulation (1) requires enforcing the following constraints (see Appendix A)

$$\sum_{d \in \mathcal{D}(c)} (\sigma^n_{cd} \boldsymbol{s}^n_{cd} - \sigma^n_{dc} \boldsymbol{s}^n_{dc}) = \boldsymbol{0}, \tag{6a}$$

$$\sum_{d \in \mathcal{D}(c)} \sigma^n_{cd} \boldsymbol{s}^n_{cd} \otimes \delta \boldsymbol{x}^n_{cd} = V^n_c \, \mathbf{I}, \tag{6b}$$

where $\delta \boldsymbol{x}^n_{cd} := \boldsymbol{x}^n_d - \boldsymbol{x}^n_c$ and $\mathbf{I}$ is the identity matrix.

Condition (6a) is trivially ensured in a finite volumes setting where $\boldsymbol{s}^n_{cd}$ are the cell face vectors—normal to faces with magnitude given by face area—and if the the upwinding factors are consistent, that is if $\sigma^n_{cd} + \sigma^n_{dc} = 1$ for any couple cd. Under these conditions, (6a) reduces to the trivial identity

$$\sum_d \boldsymbol{s}^n_{cd} = 0. \tag{7}$$

Now, condition (6b) is far less trivial even in a finite element setting and is strongly dependent on the cell shapes and sizes. As visible from (19) in Appendix A, the condition is fulfilled with a *uniform upwinding factor* and a *uniform Cartesian mesh* of squares or cubes in 2 or 3D. It is to be noted however, that conditions (6) are always *invariant* by both *affine transformations* and *convex linear combinations* of transport schemes.

The approach in the present work is to find the (possibly) best discretization to first order of the Eulerian transport operator within the framework defined by (2), (5), and (7), and complemented by (6b) whenever possible. It can be noticed that Vazquez-Gonzalez (2016) used the same formalism on a structured (but non Cartesian and non uniform) mesh. This paper goes further by exploiting the freedom left in (6) to improve transport isotropy.

3. Co-mesh approach in 2D

Usual 2D Cartesian 5-point stencils of finite volume schemes only take into account first nearest neighbors (across cell faces). In the present work so-called *co-meshes* (as described in section 3.1) are introduced in order to deal with corner fluxes through second nearest neighbors (across cell corners).

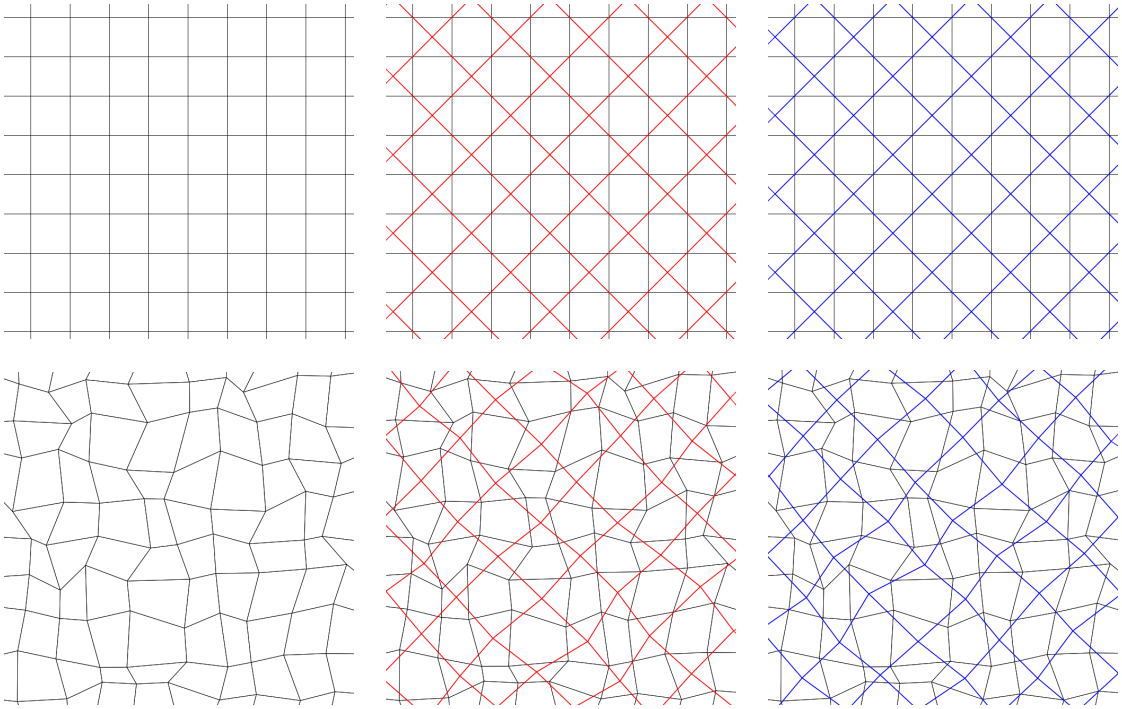

Fig. 2 Meshes and the corresponding co-meshes. Cartesian grid (top) and randomly distorted quadrilateral grid (bottom).

3.1 Construction of the co-mesh

The co-mesh represents a fictive grid that links second nearest neighbors (neighbors across cell corners in the initial mesh) through fictive cell faces (see Fig. 1). Notably, the co-mesh defines the vectors $\boldsymbol{s}_{cd}^{(2)}$ as its face normals, whereas $\boldsymbol{s}_{cd}^{(1)}$ are the face normals of the initial mesh. A cell of the co-mesh is called a *co-cell*. Each co-cell is built from the cell centers of the first nearest neighbors, where these cell centers act as the nodes of the co-mesh. This results in two co-meshes for a structured 2D grid, as shown in Fig. 2. The main idea behind this construction is to build a mesh, on top of the initial one, which omits the numerical information of the first nearest neighbors. Fig. 3b illustrates the volume of the co-cells and how the omitted parts prevent the co-mesh from having "holes" in it, in order to result in a well-defined mesh. At the moment, the co-mesh strategy is applied only to quadrilateral (but not necessarily Cartesian) structured grids. It is not clear yet how this method will be adaptable to unstructured grids.

Let us remark at this point the importance of computing the cell volumes of the co-meshes $V_c^{(i)}$ exactly, in order to preserve conservation. Considering $V_c^{(2)} = 2V_c^{(1)}$ is of course true in the case of Cartesian meshes. However, this estimate is almost surely wrong in the case of more general meshes and violates conservation as illustrated in Fig. 6.

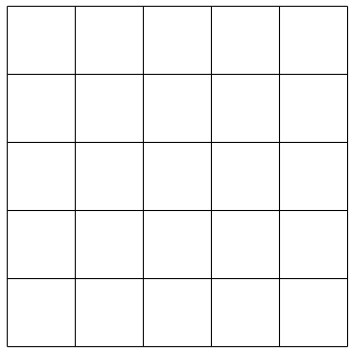

3a

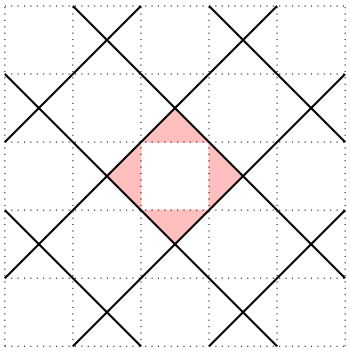

3b

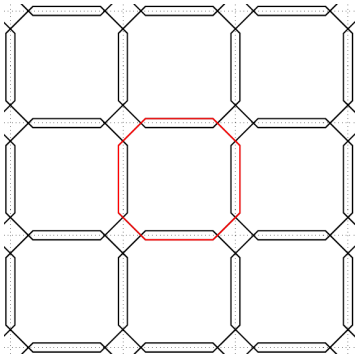

3c

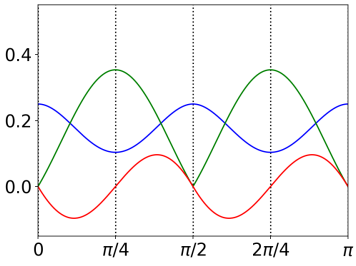

4a

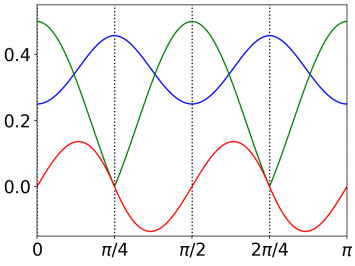

4b

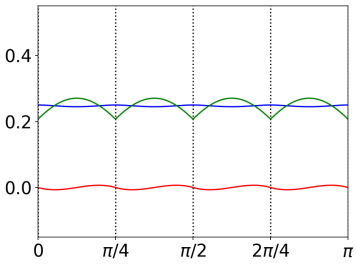

4c

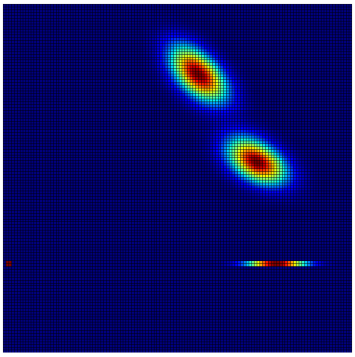

5a

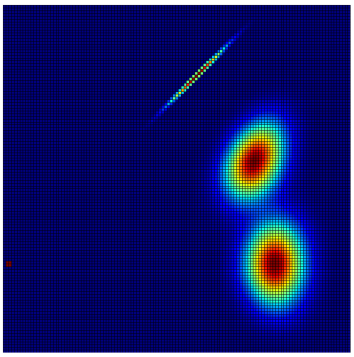

5b

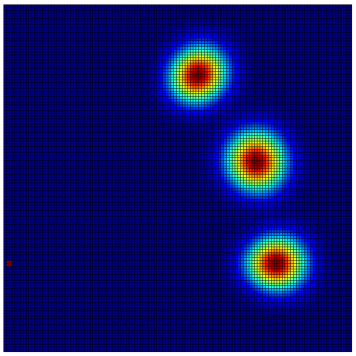

5c

Results for three different schemes given by: $\omega = 1$ (a), $\omega = 0$ (b), and ω_{opt} (c):

Fig. 3 Initial Cartesian grid (a) and *co-mesh* (b). Applying the co-mesh strategy is equivalent to applying the initial transport operator on a non-tailing but volume-preserving octagonal grid (c).

Fig. 4 Graph of the dimensionless coefficients of matrix M in basis $\{\boldsymbol{e}, \boldsymbol{e}_\perp\} = \{\frac{\boldsymbol{v}}{\|\boldsymbol{v}\|}, \boldsymbol{e}_\perp\}$ as a function of transport direction θ: $\boldsymbol{e} \cdot \mathbf{M} \cdot \boldsymbol{e}$ (blue), $\boldsymbol{e}_\perp \cdot \mathbf{M} \cdot \boldsymbol{e}_\perp$ (green), and $\boldsymbol{e} \cdot \mathbf{M} \cdot \boldsymbol{e}_\perp$ (red), scaled by $h\|\boldsymbol{v}\|$.

Fig. 5 Representation of numerical diffusion on the transport of a "delta" function (four cells at bottom left corner) along directions $\boldsymbol{v} = \|\boldsymbol{v}\|(\cos\theta, \sin\theta)$, for $\theta = 0$, $\pi/8$, and $\pi/4$; transport over a radius of $96h$ (where h is the spatial discretization step), on a 128×128 grid, in 192 iterations, with CFL $= 0.5$.

3.2 General method

The co-mesh approach consists in solving transport terms of a numerical scheme over an initial mesh and several related co-meshes (introduced in section 3.1) and linearly combine the resulting schemes $\omega \times$ scheme $+ (1-\omega) \times$ co-scheme with weight ω. This leads to a 9-point stencil on a fictive mesh as represented in Fig. 1.

The notation for the transport operator in (2) is not changed; only the neighborhood of cell c is redefined as

$$\mathcal{D}(c) = \mathcal{D}_1(c) \cup \mathcal{D}_2(c), \tag{8}$$

where $\mathcal{D}_1(c)$ and $\mathcal{D}_2(c)$ are the sets of respectively first and second nearest neighbors, and vectors $\boldsymbol{s}_{cd}$ are weighted with linear factors ω and $(1-\omega)$ as

$$\boldsymbol{s}_{cd} = \begin{cases} \omega \boldsymbol{s}_{cd}^{(1)} & \text{if} \quad d \in \mathcal{D}_1(c), \\ (1-\omega)\boldsymbol{s}_{cd}^{(2)} & \text{if} \quad d \in \mathcal{D}_2(c). \end{cases} \tag{9}$$

Hence, the co-mesh method applied to the first-order transport scheme $\mathrm{D}_{\Delta t} a_c^n = 0$ on an Eulerian grid (i.e. $V_c^{n+1} = V_c^n =: V_c = \omega V_c^{(1)} + (1-\omega) V_c^{(2)}$) writes

$$\frac{a_c^{n+1} - a_c^n}{\Delta t^n} + \frac{1}{V_c} \sum_{\substack{i=1,2 \\ d \in \mathcal{D}_i(c)}} \left(a_c^n \mathring{V}_{cd}^{(i),n} - a_d^n \mathring{V}_{dc}^{(i),n} \right) = 0, \tag{10}$$

where $\mathcal{D}_1(c)$ and $\mathcal{D}_2(c)$ are the set of first and second nearest neighbors respectively, and the superscripts (1) and (2) indicate initial and co-mesh. In other words, the geometry of the co-mesh defines the coefficients of the second nearest neighbors in the stencil.

3.3 Reducing anisotropy

The co-mesh strategy aims at reducing anisotropy. In order to find the most isotropic transport, we seek the value of ω leading to some minimal measure of anisotropy. Here, the modified equation (Warming and Hyett 1974) is used to study numerical dissipation of (10) and to determine ω. The modified equation is the equation that is actually solved to higher order by a first-order scheme of a given initial equation. It writes

$$(\partial_t a)_c^n + v_x \partial_x a_c^n + v_y \partial_y a_c^n = \left(M_{xx} (\partial_{xx}^2 a)_c^n + 2 M_{xy} (\partial_{xy}^2 a)_c^n + M_{yy} (\partial_{yy}^2 a)_c^n \right) \tag{11a}$$

$$=: \begin{pmatrix} \partial_x \\ \partial_y \end{pmatrix}^t \mathbf{M}(\boldsymbol{v}) \begin{pmatrix} \partial_x \\ \partial_y \end{pmatrix} a_c^n. \tag{11b}$$

M_{xx}, M_{xy}, M_{yy} are the effective diffusive coefficients that characterize the numerical error, and depend on the magnitude and orientation of the velocity $\boldsymbol{v}$.

Consider (10) for constant transport direction $\boldsymbol{v} := \|\boldsymbol{v}\|(\cos\theta, \sin\theta)$, with $\theta \in [0, \pi/4]$. Then, the stencil is defined through cell $c = (i,j)$ and its donor cells $\mathcal{D}_1(c) = \{(i-1,j), (i,j-1)\}$ and $\mathcal{D}_2(c) = \{(i-1,j+1), (i-1,j-1)\}$. As detailed in Appendix B, the diffusion matrix on the right hand side of (11a) has coefficients

$$M_{xx} = \tfrac{1}{2}\left(1 - \tfrac{v_x \Delta t}{\Delta x}\right) v_x \Delta x, \tag{12a}$$

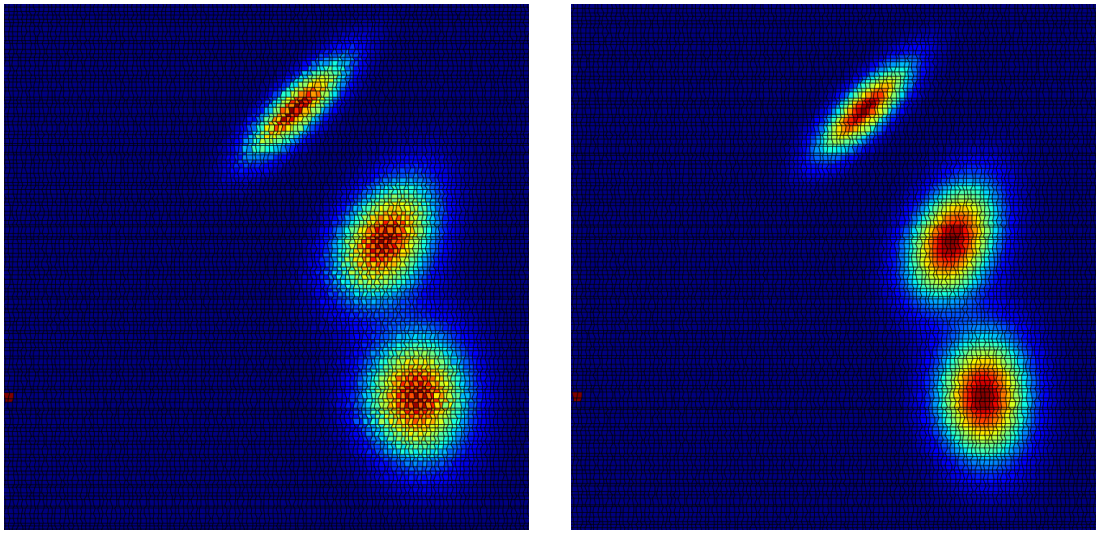

Fig. 6 Solver applied to co-mesh ($\omega = 0$). Wrong estimation of cell-volume violates conservation and monotonicity (left), compared to the correct result (right). (For details on the simulation see Fig. 5).

Table 1 Optimized values of ω for three different functionals g.

$g(\omega)$	$\|M_\times\|_\infty$	$\|M_\times - \mu(M_\times)\|_2$	$\|M_\parallel - \mu(M_\parallel)\|_2$
ω_{opt}	0.585786	0.587514	0.585863

$$M_{xy} = \tfrac{1}{2}\Big((1-\omega)v_y - \sqrt{\tfrac{v_x\Delta t}{\Delta x}\tfrac{v_y\Delta t}{\Delta y}}\sqrt{v_x v_y}\Big)\Delta x, \tag{12b}$$

$$M_{yy} = \tfrac{1}{2}\Big((1-\omega)v_x + \big(\omega - \tfrac{v_y\Delta t}{\Delta y}\big)v_y\Big)\Delta x. \tag{12c}$$

Consider matrix $\mathbf{M}(\boldsymbol{v})$ taken in the basis $\{\boldsymbol{e}, \boldsymbol{e}_\perp\} = \{\frac{\boldsymbol{v}}{\|\boldsymbol{v}\|}, \boldsymbol{e}_\perp\}$, with transport direction $\boldsymbol{v} = \|\boldsymbol{v}\| \times (\cos\theta, \sin\theta)$, and transverse direction $\boldsymbol{e}_\perp = (-\sin\theta, \cos\theta)$, which writes

$$\mathbf{M}_{\boldsymbol{v}} := \begin{pmatrix} M_\parallel & M_\times \\ M_\times & M_\perp \end{pmatrix} = \begin{pmatrix} \boldsymbol{e}^t\mathbf{M}\boldsymbol{e} & \boldsymbol{e}^t\mathbf{M}\boldsymbol{e}_\perp \\ \boldsymbol{e}_\perp^t\mathbf{M}\boldsymbol{e} & \boldsymbol{e}_\perp^t\mathbf{M}\boldsymbol{e}_\perp \end{pmatrix}. \tag{13}$$

Fig. 4 shows the coefficients of matrix $\mathbf{M}_{\boldsymbol{v}}$ over transport direction defined by θ. The imbalance between these coefficients reflects the transport anisotropy of the scheme. Transport would be isotropic, if the coefficients of $\mathbf{M}_{\boldsymbol{v}}$ would not change for different transport direction defined by angle θ. Thus, reducing transport anisotropy means reducing anisotropy of $\mathbf{M}_{\boldsymbol{v}}$. This is done through numerical optimization by minimizing some functional $g(\omega) = \|f_\omega(\theta)\|$, that describes transport anisotropy of $\mathbf{M}_{\boldsymbol{v}}$ depending on ω. Thus, minimizing over ω leads to an optimal value

$$\omega_{\text{opt}} := \arg\min_{\omega\in[0,1]} g(\omega) = \arg\min_{\omega\in[0,1]} \|f_\omega(\theta)\|. \tag{14}$$

Table 1 shows the optimal ω computed for different minimization functionals $g(\omega)$, where μ is the mean value over interval $(0, \pi/4)$. The results for ω_{opt} are very similar for these norms. However,

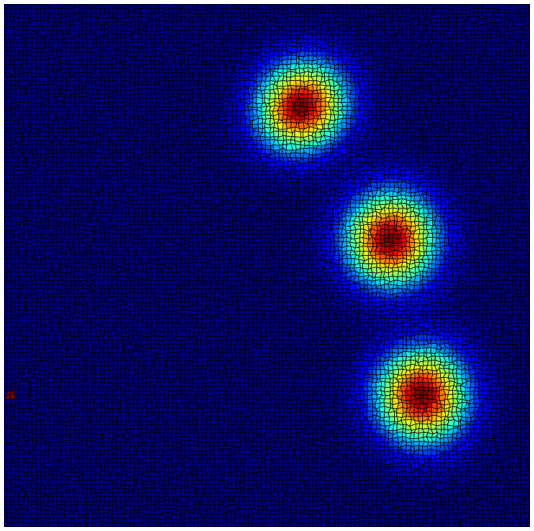

Fig. 7 Co-mesh strategy applied to a randomly distorted quadrilateral grid with ω_{opt} (details on the simulation are provided in Fig. 5).

minimizing coefficient $M_\times$ in the L^∞ norm seems to be the most ideal choice. From now on, the present work refers to the optimal value as $\omega_{\text{opt}} = \arg\min_{\omega\in[0,1]} \|M_\times\|_\infty \approx 0.585786$. Fig. 5c and 7 show the co-mesh strategy with ω_{opt} applied to the Cartesian grid and a randomly distorted quadrilateral grid.

4. Conclusion

The generic formulation for the discrete Eulerian transport operator has been introduced. A consistent version has been deduced on the co-mesh approach. The co-mesh strategy leads to improved isotropy for ω_{opt}, as visible by comparing Fig. 5a to 5c. The co-mesh approach has been introduced on usual 2D Cartesian, and distorted quadrilateral structured grids. Transport anisotropy is reduced on all of these general quadrilateral structured grids, where first-order consistency is guaranteed on 2D Cartesian, and uniformly distorted Cartesian grids (i.e. grids of identical parallelograms).

Applying the co-mesh strategy to 3D needs some further considerations. It is not obvious how this would work, especially because difficulties arise by introducing third nearest neighbors. However, it is immanent for a 3D extension, that the meshes for first to third nearest neighbors are respectively built from hexahedra, rhombic dodecahedra, and truncated octahedra in order to respect tessellation.

The co-mesh strategy has been tested on first-order transport on an Eulerian grid. It can be readily inserted in a GEEC approach, which defines a quasi-symplectic ALE scheme and requires a consistent formulation of the transport operator for mass, momentum and internal energy equations. A second-order extension is also being investigated.

A. First-order expansion and consistency conditions

This paragraph provides the derivation of consistency conditions (6) for the first-order discretization (2) of the transport operator (1). Some details on the special case of Cartesian meshes are also provided.

First-order Taylor expansions in time around t^n and space around center of mass $\boldsymbol{x}_c^n$ of cell c give

$$V_c^{n+1} = V_c^n + \Delta t\ \partial_t V_c^n + \mathcal{O}(\Delta t^2), \tag{15a}$$

$$a_c^{n+1} = a_c^n + \Delta t\ (\partial_t a)_c^n + \mathcal{O}(\Delta t^2), \tag{15b}$$

$$a_d^n = a_c^n + \delta\boldsymbol{x}_{cd}^n \cdot (\boldsymbol{\nabla} a)_c^n + \mathcal{O}(||\delta\boldsymbol{x}||^2), \tag{15c}$$

$$\boldsymbol{v}_q = \boldsymbol{v}_c^n + \delta\boldsymbol{x}_{cq}^n \cdot (\boldsymbol{\nabla} \otimes \boldsymbol{v})_c^n + \mathcal{O}(||\delta\boldsymbol{x}||^2), \tag{15d}$$

where $\delta\boldsymbol{x}_{cd}^n := \boldsymbol{x}_d^n - \boldsymbol{x}_c^n$ and $\delta\boldsymbol{x}_{cq}^n := \boldsymbol{x}_q^n - \boldsymbol{x}_c^n$. Combining these expressions and with the definition of $\mathring{V}_{dc}^n$ in (3), the first-order expansion of the transport scheme (2) is

$$\begin{aligned}(\partial_t a)_c^n + \frac{\partial_t V_c^n}{V_c^n} a_c^n \\ + \frac{1}{V_c^n}\boldsymbol{v}_c^n \cdot \sum_{d,q} (\boldsymbol{s}_{cdq}^n - \boldsymbol{s}_{dcq}^n) a_c^n + \frac{1}{V_c^n}\sum_{d,q} \delta\boldsymbol{x}_{cq}^n \cdot (\boldsymbol{\nabla}\otimes\boldsymbol{v})_c^n \cdot (\boldsymbol{s}_{cdq}^n - \boldsymbol{s}_{dcq}^n) a_c^n \\ + \frac{1}{V_c^n}\sum_{d,q} -\boldsymbol{v}_c^n \cdot \boldsymbol{s}_{dcq}^n\ \delta\boldsymbol{x}_{cd}^n \cdot (\boldsymbol{\nabla} a)_c^n = \mathcal{O}(\Delta t, ||\delta\boldsymbol{x}||),\end{aligned} \tag{16}$$

where for simplicity the upwinding factors σ_{cdq} have been omitted (i.e. $\sigma_{cdq}\boldsymbol{s}_{dcq} \to \boldsymbol{s}_{dcq}$) and sums on d or q are now restricted by setting $\boldsymbol{s}_{cdq} = 0$ whenever $d \notin \mathcal{D}(c)$ or $q \notin \mathcal{Q}(c)$.

Now, the the Eulerian transport operator can be decomposed as $\mathrm{D}_t a = \partial_t a + a\boldsymbol{\nabla}\cdot\boldsymbol{w} + \boldsymbol{\nabla}\cdot(a\boldsymbol{v}) = \partial_t a + a\boldsymbol{\nabla}\cdot\boldsymbol{w} + a\boldsymbol{\nabla}\cdot\boldsymbol{v} + \boldsymbol{v}\cdot\boldsymbol{\nabla} a$, and thus term to term identification to first order with (16) yields

$$\frac{\partial_t V_c^n}{V_c^n} a_c^n = a_c^n (\boldsymbol{\nabla}\cdot\boldsymbol{w})_c^n, \tag{17a}$$

$$\frac{1}{V_c^n}\sum_{d,q} \boldsymbol{v}_c^n \cdot (\boldsymbol{s}_{cdq}^n - \boldsymbol{s}_{dcq}^n)\ a_c^n = 0, \tag{17b}$$

$$\frac{1}{V_c^n}\sum_{d,q} \delta\boldsymbol{x}_{cq}^n \cdot (\boldsymbol{\nabla}\otimes\boldsymbol{v})_c^n \cdot (\boldsymbol{s}_{cdq}^n - \boldsymbol{s}_{dcq}^n)\ a_c^n = a_c^n (\boldsymbol{\nabla}\cdot\boldsymbol{v})_c^n, \tag{17c}$$

$$\frac{1}{V_c^n}\sum_{d,q} -(\boldsymbol{v}_c^n \cdot \boldsymbol{s}_{dcq}^n)\ (\delta\boldsymbol{x}_{cd}^n \cdot (\boldsymbol{\nabla} a)_c^n) = \boldsymbol{v}_c^n \cdot (\boldsymbol{\nabla} a_c)^n. \tag{17d}$$

As these conditions must hold whatever the transported field a and the transport velocity v—that is whatever a_c^n, $(\boldsymbol{\nabla} a)_c^n$, $\boldsymbol{v}_c^n$, and $(\boldsymbol{\nabla}\otimes\boldsymbol{v})_c^n$,—they simplify into

$$\partial_t V_c^n = V_c^n\ (\boldsymbol{\nabla}\cdot\boldsymbol{w})_c^n, \tag{18a}$$

$$\sum_{d,q}(\boldsymbol{s}^n_{cdq} - \boldsymbol{s}^n_{dcq}) = \mathbf{0}, \tag{18b}$$

$$\sum_{d,q}(\boldsymbol{s}^n_{cdq} - \boldsymbol{s}^n_{dcq}) \otimes \delta\boldsymbol{x}^n_{cq} = V^n_c\ \mathbf{I}, \tag{18c}$$

$$\sum_{d,q} -\boldsymbol{s}^n_{dcq} \otimes \delta\boldsymbol{x}^n_{cd} = V^n_c\ \mathbf{I}, \tag{18d}$$

where $\mathbf{I}$ is the identity matrix. The grid evolution always complies with (18a) (it is the so-called GCL condition) thus only the last three conditions need to be retained.

When further restricting the velocity discretization by setting the set of points $\boldsymbol{x}_q$ equal to the single point $\boldsymbol{x}_c$ in $\mathring{V}_{dc}$, conditions (18c) and (18d) become identical and, reintroducing the upwinding factors, the final two conditions provided in (6) are obtained.

In the case of a 2D Cartesian mesh with transport between adjacent cells, constraint (18d) is simply expanded along x and y coordinates, and with explicit upwinding factors σ reduces to

$$\sum_{d\in\mathcal{D}(c)} \sigma_{cd} s_{cd,x} \delta x_{cd,x} = V_c, \tag{19a}$$

$$\sum_{d\in\mathcal{D}(c)} \sigma_{cd} s_{cd,y} \delta x_{cd,y} = V_c, \tag{19b}$$

$$\sum_{d\in\mathcal{D}(c)} \sigma_{cd} s_{cd,x} \delta x_{cd,y} = 0, \tag{19c}$$

$$\sum_{d\in\mathcal{D}(c)} \sigma_{cd} s_{cd,y} \delta x_{cd,x} = 0. \tag{19d}$$

It is readily observed that these conditions are fulfilled with a velocity of *uniform direction* on a *uniform* mesh: only one donor cell appears in each sum and $V_c = s_{cd}\delta x_{cd}$ for any couple of neighboring cells cd.

B. Modified equation applied to the first-order transport scheme with co-meshes

The numerical diffusion coefficients M_{xx}, M_{xy} and M_{yy} of the modified equation (11a) can be calculated by the following recipe: first the second-order expansion of the scheme is computed and then time derivatives higher than the scheme's order and mixed time and space derivatives are eliminated. The latter is a straightforward computation and can be implemented in any computer algebra system (CAS) performing symbolic computations, such as Mathematica or the Python library Sympy. However, this appendix provides some details for the calculations on scheme (10).

In order to compute the second-order residue, the corresponding Taylor expansions in time and space are introduced

$$a^{n+1}_c = a^n_c + \Delta t(\partial_t a)^n_c + \tfrac{1}{2}(\Delta t)^2(\partial^2_{tt} a)^n_c + \mathcal{O}(\Delta t^3), \tag{20a}$$

$$a^n_d = a^n_c + \delta\boldsymbol{x}^n_{cd} \cdot (\boldsymbol{\nabla} a)^n_c + \tfrac{1}{2}\delta\boldsymbol{x}^n_{cd} \cdot (\boldsymbol{\nabla}^2 a)^n_c \cdot \delta\boldsymbol{x}^n_{cd} + \mathcal{O}(||\delta\boldsymbol{x}||^3), \tag{20b}$$

with $\delta\boldsymbol{x}^n_{cd} := \boldsymbol{x}^n_d - \boldsymbol{x}^n_c$, for $d \in \mathcal{D}_i(c),\ i = 1, 2$. Furthermore, $\delta\boldsymbol{x}^n_{dc} = \boldsymbol{x}^n_c - \boldsymbol{x}^n_d = -\delta\boldsymbol{x}^n_{cd}$. Considering a Cartesian grid and a constant velocity vector $\boldsymbol{v}_d = \boldsymbol{v}_c$, the space discretization can be

simplified. Recall from section 2 that conservation of a field a is enforced over any volume V_c by constraint $\sum_{d\in\mathcal{D}(c)} \boldsymbol{s}_{cd}^n = 0$. It follows

$$\sum_{d\in\mathcal{D}(c)} \left(\mathring{V}_{cd}^n a_c^n - \mathring{V}_{dc}^n a_d^n\right) \overset{(20b)}{=} \underbrace{\sum_{d\in\mathcal{D}(c)} \underbrace{(\sigma_{cd}^n + \sigma_{dc}^n)}_{=1} \boldsymbol{s}_{cd}^n \cdot \boldsymbol{v}_c^n a_c^n}_{=0} - \sum_{d\in\mathcal{D}(c)} \sigma_{dc}^n \boldsymbol{s}_{dc}^n \cdot \boldsymbol{v}_c^n \Big(\delta\boldsymbol{x}_{cd}^n \cdot (\boldsymbol{\nabla} a)_c^n + \tfrac{1}{2}\delta\boldsymbol{x}_{cd}^n \cdot (\boldsymbol{\nabla}^2 a)_c^n \cdot \delta\boldsymbol{x}_{cd}^n\Big). \quad (21)$$

A simple computation shows that (18d) is valid on the Cartesian mesh and its co-mesh. Therefore, the following term on the right hand side of (21) can be simplified in this case and becomes

$$-\sum_{\substack{i=1,2\\ d\in\mathcal{D}_i(c)}} \sigma_{dc}^{(i)} (\boldsymbol{s}_{dc}^{(i)} \cdot \boldsymbol{v}_c)\ \delta\boldsymbol{x}_{cd}^n \cdot (\boldsymbol{\nabla} a)_c^n = \omega V_c^{(1)} \boldsymbol{v}_c \cdot (\boldsymbol{\nabla} a)_c^n + (1-\omega) V_c^{(2)} \boldsymbol{v}_c \cdot (\boldsymbol{\nabla} a)_c^n = V_c \boldsymbol{v}_c \cdot (\boldsymbol{\nabla} a)_c^n. \quad (22)$$

Then, the second-order expansion writes

$$(\partial_t a)_c^n + \boldsymbol{v}_c \cdot (\boldsymbol{\nabla} a)_c^n = -\tfrac{1}{2}\Delta t (\partial_{tt}^2 a)_c^n + \frac{1}{V_c} \sum_{\substack{i=1,2\\ d\in\mathcal{D}_i(c)}} \sigma_{dc}^{(i)} \boldsymbol{s}_{dc}^{(i)} \cdot \boldsymbol{v}_c \big(\tfrac{1}{2}\delta\boldsymbol{x}_{cd}^n \cdot (\boldsymbol{\nabla}^2 a)_c^n \cdot \delta\boldsymbol{x}_{cd}^n\big). \quad (23)$$

The modified equation is obtained by eliminating the second-order time derivative in (23). $(\partial_{tt}^2 a)_c^n$ is given by differentiation of (23) in time. In this expression the mixed time and space derivatives $(\partial_{tx}^2 a)_c^n$ and $(\partial_{ty}^2 a)_c^n$ appear, which can be eliminated by differentiation of (23) in each spatial direction. Remark that the computations in (19) are valid on the co-mesh of a Cartesian grid, which is used in the following calculations.

$$(\partial_{tt}^2 a)_c^n = \frac{1}{V_c} \sum_{\substack{i=1,2\\ d\in\mathcal{D}_i(c)}} \sigma_{dc}^{(i)} \boldsymbol{s}_{dc}^{(i)} \cdot \boldsymbol{v}_c \big(\delta x_{cd,x} (\partial_{tx}^2 a)_c^n + \delta x_{cd,y} (\partial_{ty}^2 a)_c^n\big) \overset{(19)}{=} -v_x (\partial_{tx}^2 a)_c^n - v_y (\partial_{ty}^2 a)_c^n, \quad (24a)$$

$$(\partial_{tx}^2 a)_c^n = \frac{1}{V_c} \sum_{\substack{i=1,2\\ d\in\mathcal{D}_i(c)}} \sigma_{dc}^{(i)} \boldsymbol{s}_{dc}^{(i)} \cdot \boldsymbol{v}_c \big(\delta x_{cd,x} (\partial_{xx}^2 a)_c^n + \delta x_{cd,y} (\partial_{xy}^2 a)_c^n\big) \overset{(19)}{=} -v_x (\partial_{xx}^2 a)_c^n - v_y (\partial_{xy}^2 a)_c^n, \quad (24b)$$

$$(\partial_{ty}^2 a)_c^n = \frac{1}{V_c} \sum_{\substack{i=1,2\\ d\in\mathcal{D}_i(c)}} \sigma_{dc}^{(i)} \boldsymbol{s}_{dc}^{(i)} \cdot \boldsymbol{v}_c \big(\delta x_{cd,x} (\partial_{xy}^2 a)_c^n + \delta x_{cd,y} (\partial_{yy}^2 a)_c^n\big) \overset{(19)}{=} -v_x (\partial_{xy}^2 a)_c^n - v_y (\partial_{yy}^2 a)_c^n, \quad (24c)$$

and therefore

$$(\partial_{tt}^2 a)_c^n = v_x^2 (\partial_{xx}^2 a)_c^n + 2 v_x v_y (\partial_{xy}^2 a)_c^n + v_y^2 (\partial_{yy}^2 a)_c^n. \quad (25)$$

Hence, the coefficients of the modified equation (11a) write

$$2M_{xx} = -\Delta t v_x^2 + \frac{1}{V_c} \sum_{\substack{i=1,2\\ d\in\mathcal{D}_i(c)}} \sigma_{dc}^{(i)} \boldsymbol{s}_{dc}^{(i)} \cdot \boldsymbol{v}_c\ \delta x_{cd,x}^2, \quad (26a)$$

$$2M_{xy} = -\Delta t v_x v_y + \frac{1}{V_c}\sum_{\substack{i=1,2\\ d\in\mathcal{D}_i(c)}} \sigma_{dc}^{(i)} \boldsymbol{s}_{dc}^{(i)} \cdot \boldsymbol{v}_c \, \delta x_{cd,x}\delta x_{cd,y}, \tag{26b}$$

$$2M_{yy} = -\Delta t v_y^2 + \frac{1}{V_c}\sum_{\substack{i=1,2\\ d\in\mathcal{D}_i(c)}} \sigma_{dc}^{(i)} \boldsymbol{s}_{dc}^{(i)} \cdot \boldsymbol{v}_c \, \delta x_{cd,y}^2. \tag{26c}$$

C. Anisotropy and CFL

Consider constant velocity vector $\boldsymbol{v}_d = \boldsymbol{v}_c$. In this case, there are eight possible sets of active donor cells. These sets are defined through the intervals $I_k = [\frac{k\pi}{4}, \frac{(k+1)\pi}{4}]$, for $k \in \mathbb{Z}/8\mathbb{Z}$. Choose for instance transport direction $\boldsymbol{v} = \|\boldsymbol{v}\|(\cos\theta, \sin\theta)$, with $\theta \in [0, \frac{\pi}{4}]$, then on the Cartesian mesh, where $\delta x_x = \delta x_y =: \Delta x$, the numerical diffusion matrix defined in (11b) writes

$$\mathbf{M}(\boldsymbol{v}) = \tfrac{1}{2}\Delta x \begin{pmatrix} v_x & (1-\omega)v_y \\ (1-\omega)v_y & (1-\omega)v_x + \omega v_y \end{pmatrix} + \mathbf{M}_{\text{CFL}}, \qquad \theta \in [0, \pi/4], \tag{27}$$

with

$$\mathbf{M}_{\text{CFL}} = -\frac{\Delta t}{\Delta x}\begin{pmatrix} v_x^2 & v_x v_y \\ v_x v_y & v_y^2 \end{pmatrix} \tag{28}$$

Remark that the coefficients of $\mathbf{M}(\boldsymbol{v})$ change for the different sets of donor cells symmetrically. Fig. 4a to 4c illustrate the symmetries of $\mathbf{M}(\boldsymbol{v})$ in basis $\{\boldsymbol{e}, \boldsymbol{e}_\perp\}$ over I_0 to I_3.

Recall the representation of matrix $\mathbf{M}$ in basis $\{\boldsymbol{e}, \boldsymbol{e}_\perp\} = \{\frac{\boldsymbol{v}}{\|\boldsymbol{v}\|}, \boldsymbol{e}_\perp\}$, noted $\mathbf{M}_{\boldsymbol{v}}$, with transport direction $\boldsymbol{v} = \|\boldsymbol{v}\|(\cos\theta, \sin\theta)$, and transverse direction $\boldsymbol{e}_\perp = (-\sin\theta, \cos\theta)$.

$$\mathbf{M}_{\boldsymbol{v}} = \begin{pmatrix} M_\parallel & M_\times \\ M_\times & M_\perp \end{pmatrix} = \begin{pmatrix} \boldsymbol{e}\cdot\mathbf{M}\cdot\boldsymbol{e} & \boldsymbol{e}\cdot\mathbf{M}\cdot\boldsymbol{e}_\perp \\ \boldsymbol{e}\cdot\mathbf{M}\cdot\boldsymbol{e}_\perp & \boldsymbol{e}_\perp\cdot\mathbf{M}\cdot\boldsymbol{e}_\perp \end{pmatrix}. \tag{29}$$

The following calculations show that the representation of this matrix in basis $\{\boldsymbol{e}, \boldsymbol{e}_\perp\}$ does not depend on the CFL up to a linear term (and this only for coefficient $M_\parallel$), as the coefficients of $\mathbf{M}_{\boldsymbol{v},\text{CFL}}$ are constant over θ.

$$M_{\parallel,\text{CFL}} = \boldsymbol{e}\cdot\mathbf{M}_{\text{CFL}}\cdot\boldsymbol{e} = -\frac{\Delta t}{\Delta x}\big(v_x^4 + 2v_x^2v_y^2 + v_y^4\big) = -\frac{\Delta t}{\Delta x}\big(\underbrace{v_x^2 + v_y^2}_{=\cos^2\theta+\sin^2\theta=1}\big)^2 = -\frac{\Delta t}{\Delta x}, \tag{30a}$$

$$M_{\times,\text{CFL}} = \boldsymbol{e}\cdot\mathbf{M}_{\text{CFL}}\cdot\boldsymbol{e}_\perp = -\frac{\Delta t}{\Delta x}\big(\underbrace{v_x^3 v_{x_\perp} + v_x v_y (v_x v_{y_\perp} + v_{x_\perp} v_y) + v_y^3 v_{y_\perp}}_{=\sin\theta\cos\theta(-\cos^2\theta+\cos^2\theta-\sin^2\theta+\sin^2\theta)=0}\big) = 0, \tag{30b}$$

$$\begin{aligned} M_{\perp,\text{CFL}} = \boldsymbol{e}_\perp\cdot\mathbf{M}_{\text{CFL}}\cdot\boldsymbol{e}_\perp &= -\frac{\Delta t}{\Delta x}\big(v_x^2 v_{x_\perp}^2 + 2v_x v_{x_\perp} v_y v_{y_\perp} + v_y^2 v_{y_\perp}^2\big) \\ &= -\frac{\Delta t}{\Delta x}\big(\underbrace{v_x v_y + v_{x_\perp} v_{y_\perp}}_{=-\cos\theta\sin\theta+\sin\theta\cos\theta=0}\big)^2 = 0. \end{aligned} \tag{30c}$$

References

Bouche, D., Ghidaglia, J.-M. and Pascal, F. (2005), "Error estimate and the geometric corrector for the upwind finite volume method applied to the linear advection equation", *SIAM J. Numer. Anal.*, **43**(2), 578–603. https://doi.org/10.1137/040605941.

Burton, D.E., Morgan, N.R., Carney, T.C., and Kenamond, M.A. (2015), "Reduction of dissipation in Lagrange cell-centered hydrodynamics (CCH) through corner gradient reconstruction (CGR)", *J. Comput. Phys.*, **299**, 229–280. https://doi.org/10.1016/j.jcp.2015.06.041.

DeBar, R. (1974), "Fundamentals of the KRAKEN code", Report UCIR-17366, Lawrence Livermore National Laboratory. https://doi.org/10.2172/7227630.

Hamilton, B. and Bilbao, S. (2013), "On finite difference schemes for the 3-D wave equation using non-Cartesian grids", *Proceedings of the Sound and Music Computing Conference*, Stockholm, Sweden.

Hirt, C.W., Amsden, A.A., and Cook, J.L. (1974), "An arbitrary Lagrangian-Eulerian computing method for all flow speeds", *J. Comput. Phys.*, **14**(3), 227–253. https://doi.org/10.1016/0021-9991(74)90051-5.

Kumar, A. (2004), "Isotropic finite-differences", *J. Comput. Phys.*, **201**(1), 109–118. https://doi.org/10.1016/j.jcp.2004.05.005.

Lung, T.B. and Roe, P.L. (2012), "Toward a reduction of mesh imprinting", *Int. J. Numer. Methods Fluids*, **76**(7), 450–470. https://doi.org/10.1002/fld.3941.

Potter, M.E., Lamoureux, M., and Nauta, M.D. (2011), "An FDTD scheme on a face-centered-cubic (FCC) grid for the solution of the wave equation", *J. Comput. Phys.*, **18**, 53–80. https://doi.org/10.1016/j.jcp.2011.04.027.

Roe, P. (2017), "Multidimensional upwinding", *Handbook of Numerical Analysis*, **18**, 53–80. https://doi.org/10.1016/bs.hna.2016.10.009.

Salmasi, M. and Potter, M. (2018), "Discrete exterior calculus approach for discretizing Maxwell's equations on face-centered cubic grids for FDTD", *J. Comput. Phys.*, **364**, 298–313. https://doi.org/10.1016/j.jcp.2018.03.019.

Terekhov, K.M., Mallison, B.T., and Tchelepi, H.A. (2017), "Cell-centered nonlinear finite-volume methods for the heterogeneous anisotropic diffusion problem", *J. Comput. Phys.*, **330**, 245–267. https://doi.org/10.1016/j.jcp.2016.11.010.

Vazquez-Gonzalez, T. (2016), "Conservative and mimetic numerical schemes for compressible multiphase flows simulation", Ph.D. dissertation, Université Paris-Saclay, France. https://www.theses.fr/2016SACLC051.

Warming, R.F. and Hyett, B.J. (1974), "The modified equation approach to the stability and accuracy analysis of finite-difference methods", *J. Comput. Phys.*, **14**(2), 159–179. https://doi.org/10.1016/0021-9991(74)90011-4.

Zohuri B. (2017), "Inertial Confinement Fusion Driven Thermonuclear Energy", *Springer*. https://doi.org/10.1007/978-3-319-50907-5.